RESEARCH PAPER

Constant *V/f* Control and Frequency Control of Isolated Winding Induction Motor Using Nine-Level Three-Phase Inverter

Bidyut Mahato[1] · K. C. Jana[1] · P. R. Thakura[2]

Abstract

Modern industrial applications deal with power conversion system with lesser harmonic content for variable voltage and variable frequency application. In this paper, a generalized multilevel inverter has been proposed with nearest level modulation technique. A nine-level asymmetrical inverter of 5 kW has been developed as laboratory prototype and tested with three-phase isolated winding induction motor of rating 1 HP, 200 V, 50 Hz. Unlike any other control technique, the output voltage levels remain fixed at different modulation indexes using nearest level modulation technique, thereby reducing the harmonic content, switching losses and total harmonic distortion. In this paper, a DC–DC converter stage is used to control the DC link voltage of inverter for variable speed application. AC link system (a multiwinding transformer–rectifier) and a closed-loop voltage control technique are used to obtain multiple variable DC voltage sources. A single DC source is used for constant *V/f* control and frequency control of induction motor, i.e. isolated or open-end winding at above base speed as well as below base speeds. Simulation results of phase voltage of stator terminal, phase current of stator terminal, speed and torque are shown at different speeds. The experimental results of output voltages at different speeds for constant *V/f* control and frequency control are recorded as well. The experiment is carried out at different stator voltages (or stator frequencies) below and above the rated speed, and a few experimental results are presented. The numbers of inverter voltage levels are always same, and hence, their total harmonic distortion also remains nearly constant at different speeds of operation.

Keywords Multilevel inverter · Nearest level modulation strategy · Induction motor drive · Variable DC link voltage · DC–DC power conversion

1 Introduction

In the late 1990s, gate-commutated thyristors and high-power IGBTs (insulated-gate bipolar transistors) became popular amongst the power switching devices (Lai and Peng 1996; Rodríguez et al. 2002; Bhuvaneswari and Nagaraju 2005), and IGCTs (integrated gate-commutated thyristors) are now extensively used in various applications in drives for medium-voltage control (Mahato et al. 2014), industrial motor control in traction system, chemical industry and oil industry due to ease of gate control, snubberless operation, superior switching characteristics and reduced power losses (Krug et al. 2007). The main objective of the multilevel converter is to synthesize a sinusoidal voltage of several levels obtained from capacitor voltage sources (Wen and Smedley 2008). As the number of levels increases, total harmonic distortion (THD) in the output voltage waveform is reduced, resulting in less switching losses (Al-Othman and Abdelhamid 2009). The multilevel voltage source inverters (VSIs) have recently been used in many industrial, subway applications (Dixon and Morán 2005) and also employed in power quality improvement including HVDC, AC power supplies, static VAR compensators, STATCOM (Sudheer and Prasad 2014), drive systems and renewable energy sources (Abu-rub et al. 2010; Rodríguez et al. 2007, 2009). Basic multilevel inverter is classified as: (1) diode clamped, (2) flying

✉ Bidyut Mahato
  bidyut_mahato@ee.ism.ac.in

[1] Indian Institute of Technology (Indian School of Mines), Dhanbad, India

[2] Birla Institute of Technology, Mesra, Ranchi, India

capacitor and (3) cascaded inverter topologies (Malekjamshidi et al. 2014; Franquelo et al. 2008).

Cascaded multilevel converters have (Cheng et al. 2006; Babaei and Moeinian 2010) advantages in terms of capability of fault tolerant, modular structure, minimum number of components and reliability (Lezana and Ortiz 2009; Banaei and Salary 2011). A multilevel cascaded H-bridge (CHB) structure is based on a series connection of several single-phase H-bridge inverters also called cells. The three multilevel converter structures (Rodríguez et al. 2009) such as cascaded H-bridge, neutral point clamped (NPC) and flying capacitor (FC) are capable of generating multilevel output, but they are symmetrical topologies as they are fed by equal DC sources (Colak et al. 2011). Asymmetrical multilevel inverter (MLI) is a modification of existing cascaded H-bridge structure that has advantages mainly in two manners (Hosseinzadeh et al. 2013; Ruiz-Caballero et al. 2009). Firstly, the DC input to asymmetrical multilevel inverter cells is not symmetrical but scaled in some particular ratio (Vazquez et al. 2009). Secondly, all the cells are not equally stressed in terms of power distribution. Some cells carry high power and others low power. Use of hybrid component structure such as IGCTs for high-power cells (generating low-frequency pulses) and IGBTs for lower-power cells (generating high-frequency pulses) is required for economical design (Lu et al. 2010; Rech and Pinheiro 2007). Also, the switching losses can be minimized in asymmetrical multilevel inverters as compared to conventional multilevel inverters by using appropriate PWM method.

An asymmetrical MLI for motor drive (open-end winding IM) system using a high-frequency AC link system (HFL) is presented in Dixon et al. (2010). In (Boby et al. 2016), SVPWM-based MLI for open-end winding IM is proposed to eliminate harmonics voltage (fifth and seventh) for whole modulation range. In conventional *V/f* control, voltage (stator) is controlled by controlling the DC link voltage at the inverter stage rather than by controlling the DC link voltage at converter stage unlike variable speed induction motor (IM) drives applications like traction drives. However, the fundamental frequency of the inverter can be controlled by the suitable modulation at the inverter stage (Pramanick et al. 2015; Edpuganti and Rathore 2015; Sudharshan et al. 2015). In Chowdhury et al. (2016), a multilevel converter using *V/f* operation for IM (open-end winding) drive has been presented where floating capacitor bank (half the DC link voltage) using redundant switching states is used to produce the output voltage levels.

Various PWM control strategies such as carrier-based PWM (McGrath and Holmes 2002; Naderi and Rahmati 2008), dual reference phase shifted PWM (Jana et al. 2016), space vector pulse width modulation (SVPWM) technique (Jana and Biswas 2015), selective harmonic elimination (SHE) (Dahidah et al. 2015), synchronous optimal pulse width modulation (Rathore and Edpuganti 2015) and Nearest level control (NLC) has been reported. Nearest level control is a frequently used modulation technique that has been proposed for power distribution in hybrid multicell converter (Perez et al. 2007) used in higher-power, high-level inverter applications (Li et al. 2016; Xiong et al. 2016; Hu and Jiang 2015). NLC has due advantages over SHE as it does not require calculating the firing angles, thus making calculations easier. In SVPWM technique, determining all redundant switching states and the appropriate switching sequences is the most difficult task in comparison with the analysis of NLC as elaborated in Deng and Harley (2015). In Son et al. (2012) and Meshram and Borghate (2015), a round-based nearest level control (NLC) method is demonstrated where the nearest output voltage levels are obtained by converting to the desired output voltage reference and therefore the switching states of inverter are also generated simultaneously.

In this paper, the proposed inverter keeps the entire number of voltage levels for all output voltage amplitude, if the input power source is variable. As no DC source is inherently variable in nature. So the chopper is introduced in the scheme to make the DC source variable. However, the system can also work with variable PWM; but in this case, the nearest level modulation (comparison based or algorithm based) produces voltage levels with distortion and therefore the DC supply is made variable. A novel control scheme called nearest level modulation (NLM) is proposed to realize a nine-level cascaded multilevel converter topology with only a single DC source, and the output voltage step is generated by synthesizing the voltages of both the bridges, i.e. MAIN H-bridge and the auxiliary H-bridge, whereas the switching states are separately generated for both the bridges, i.e. MAIN H-bridge and the auxiliary H-bridge.

2 Principle and Operation

For variable speed operation, the stator voltage (V_s) can be varied in proportion to the inverter frequency (f_s) so that the stator flux remains constant using the constant V/f technique. In order to develop enough torque for the induction motor at low-speed operation (Luo et al. 2006), a closed-loop slip speed estimation-based methodology is used. In conventional V/f control techniques, the voltage and frequency are controlled at the inverter stage using a pulse width modulation (PWM) technique (Luo et al. 2006; Wang and Fang 2003). However, in the proposed modulation technique, the voltage is controlled through a DC–DC converter stage and the frequency can be varied at the inverter stage using the nearest level modulation strategy,

and the overall block diagram of the proposed methodology for *V/f* scalar control of induction motor drive is shown in Fig. 1.

At the stator terminals of the three-phase induction motor, the three-phase voltages and currents can be sensed and can be converted to rotating d–q axis components. This allows the decoupling of the stator current into two parts, responsible for flux and torque components. With the known values of torque and stator current in the rotor-oriented frame, the slip speed can be estimated (Wang and Fang 2003) which is further added to the reference speed command to generate the synchronous speed. The gain of the proportional integral (PI) controller is so adjusted that the actual DC link voltage (VDC) equals the DC link command voltage ($V_{DC}*$) and hence the desired stator voltage can be achieved. For variable speed application, using the above *V/f* control, a DC link voltage control technique at the DC–DC converter stage is proposed in this paper. The command voltage of the DC–DC converter ($V_{DC}*$) proportional to the stator frequency (f_s) can be used for the closed-loop voltage control. On the other hand, for obtaining the variable frequency operation, the angle command (θ_e) can be obtained from the synchronous speed signal (ω_e), to generate the three-phase sinusoidal reference signals of unity magnitude for a nine-level asymmetrical inverter. In this proposed asymmetrical MLI configuration, the induction motor should have isolated

winding (IW) or open windings as indicated by six lines in the stator terminals as shown in Fig. 1.

The Aux H-bridges operate at low power maximally 16.67% of full drive load. The component list to configure the AC link system contains only one multiwinding transformer, a square wave inverter and some bridge rectifiers made with simple fast recovery diodes. For the asymmetrical operation of inverter, the ratio of transformer primary and secondary windings is kept as 3:1. The MAIN inverter is fed directly by the adjustable DC supply (V_{DC} or $3V_{dc}$), and all the Aux bridges are fed through transformer with reduced amplitude of DC voltage (V_{dc}). This way, all H-bridges are fed from the adjustable DC supply, and the output voltage is modified by changing the voltage of this DC supply.

2.1 AC Link System

Another main block of power circuit is AC link system. An AC link system, as illustrated in Fig. 2, mainly consists of an H-bridge inverter (square wave generator) and a multiwinding transformer and some fast operating diodes for rectification purpose. The whole modification is done to keep main DC supply to one only. All the Aux bridges (total three) are fed through AC link system as shown in Fig. 2. The variable DC supply after chopper is fed to square wave inverter which converts DC into AC. The square wave inverter is made to operate on fix duty cycle
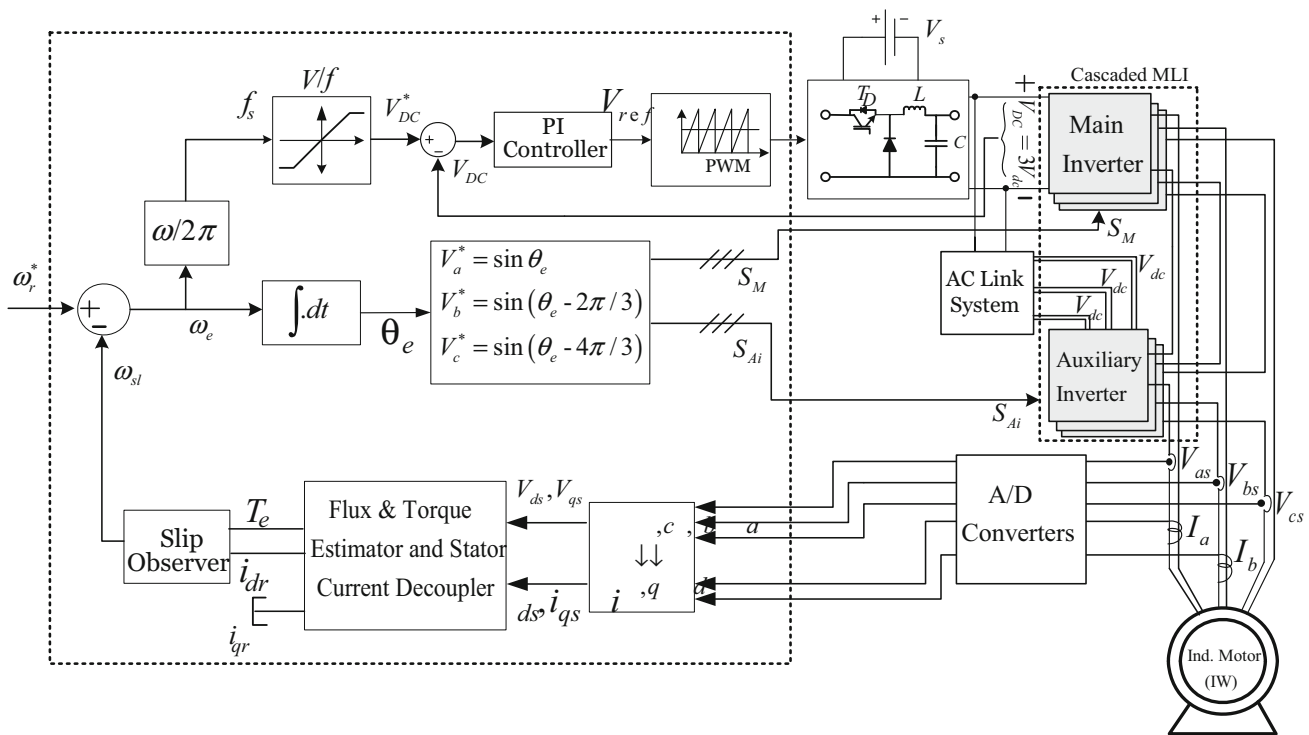

Fig. 1 Overall block diagram for proposed *V/f* control technique for the scalar control of induction motor with constant levels of the inverter
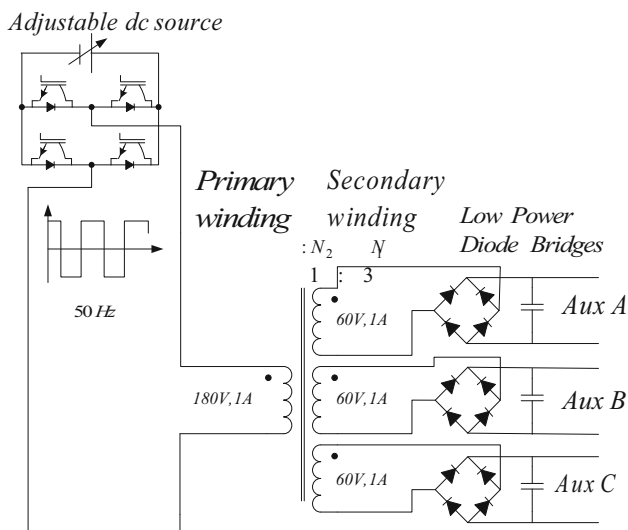
Fig. 2 Schematic diagram of AC link system using multiwinding transformer

PWM pulses at very high frequency. The output of this inverter is square wave AC output.

The AC square wave output is fed to the primary side of transformer where the primary and secondary turn ratios of the transformer are kept in scale of three, i.e. 3:1. All the secondary windings maintain the ratio of 3:1. So the output of secondary is also square waves with reduced amplitude of V_{dc}. Each of these square AC voltages is rectified using simple diode bridges. A simple diode rectifier owes its own unique benefit of absent control circuitry. This will also keep the relation 3:1 at the corresponding DC link voltages, avoiding additional voltage distortion when adjustable DC source is modified.

2.2 Nearest Level Modulation Strategy

The DC voltage of each inverter "n" is defined by $V_{dcn} = m_n V_{dc}$ where V_{dc} is a base DC link voltage and m_n is its asymmetry factor. Each inverter n is capable of generating three output voltage levels $+ m_n V_{dc}$, 0 and $- m_n V_{dc}$. The total number of output voltage levels, $L = 2N + 1$, $N = \sum_{n=1}^{N_{cell}} m_n$. When the symmetry is trinary, $m_n = 3m_n - 1$, the number of levels is maximum and is given by $L = 3^{N_{cell}}$.

Figure 3a shows the output voltage level for a two-cell hybrid converter with trinary symmetry $m_1 = 3$, $m_2 = 1$ where the total number of levels, $L = 9$, has been studied.

Considering the MAIN inverter with the higher DC link voltage ($3V_{dc}$), the voltage reference is the original modulating signal.

$$V_{r1} = m \sin(\omega t).$$

Comparing the reference signal with the constant value of K_1 and K_2 generates the switching pattern of the main and auxiliary inverter given by $K_1 = \frac{m_1}{2N}$, $K_2 = \frac{m_2}{2N}$.

Then, the switching pattern for the MAIN and Aux inverter is given by the complete algorithm for each "n" inverter cells as

$$V_{rn} = \left\{ \begin{array}{c} m \sin(\omega t)\, n = 1 \\ V_{r(n-1)} - 2K_{(n-1)}S_{(n-1)}\, n > 1 \end{array} \right\}$$

where $K_n = \dfrac{m_n}{2N}$

$$S_n = (V_{rn} > K_n) - (V_{rn} < - K_n).$$

Nearest level modulation for n level is depicted in Fig. 3a, and the formation of nine levels in a phase of load voltage with fundamental voltage waveform is shown in Fig. 3b along with the indication of the load voltage across inverter, main inverter cell and auxiliary inverter cell.

2.3 Proposed Open-Loop *V/f* Control of IM Based on Stator Decoupled Current

Compared with the superior but complex control, i.e. vector control of induction motor, *V/f* control is simple and low cost. For low-frequency range of application, the *V/f* control is not that successful and performance is also not good due to its stator resistance voltage drop and insufficient rotor slip to develop enough torque to drive the motor. A compensation methodology is presented in order to develop enough torque to start the motor with rated load torque at very low frequency (Sudharshan et al. 2015). All the estimations are done in rotor-flux-oriented frame.

2.3.1 Flux Estimator

The flux estimator calculates the estimated values of stator flux components values working along with direct axis and quadrature axis as depicted in Eq. (1). In order to find the flux components, i.e. Ψ_{ds}^s, Ψ_{qs}^s, the equations can be written as follows:

$$\left. \begin{array}{c} \Psi_{ds}^s = \int \left(v_{ds}^s - R_s i_{ds}^s \right) dt \\ \Psi_{qs}^s = \int \left(v_{qs}^s - R_s i_{qs}^s \right) dt \end{array} \right\}. \tag{1}$$

After, the stator flux and currents are calculated in stator reference frame; the motor developed electromagnetic torque shown in Eq. (2) can be estimated as,

$$T_e = \left(\frac{3}{2} \right) n_p \left(\Psi_{ds}^s i_{qs}^s - \Psi_{qs}^s i_{ds}^s \right), \tag{2}$$

where n_p = number of poles of machine and R_s = stator resistance.
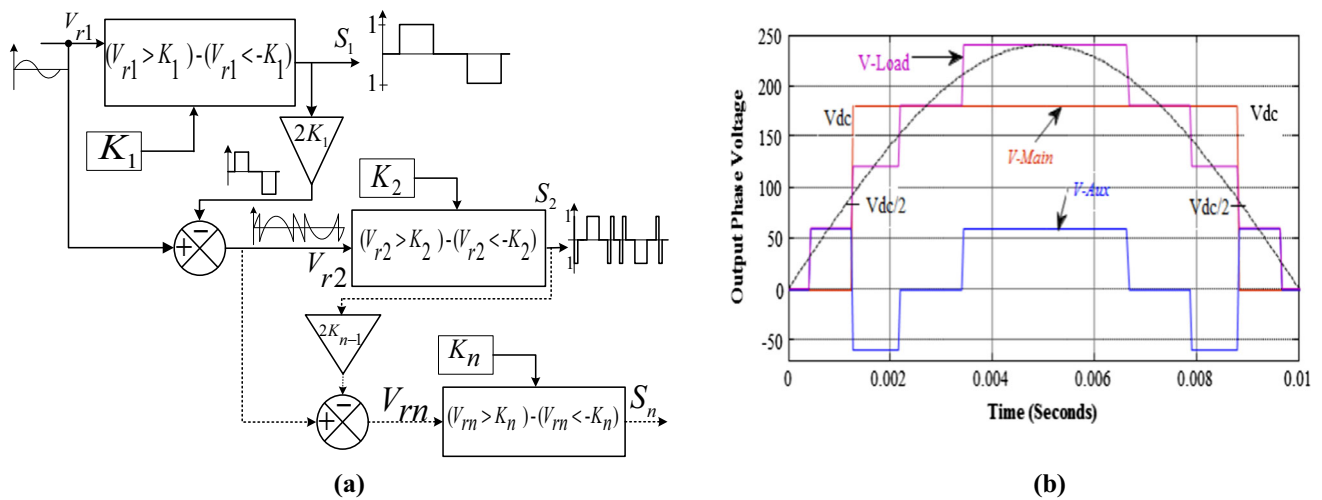
Fig. 3 **a** Nearest level modulation technique. **b** Voltage waveforms and fundamental voltages at each H-bridge

2.3.2 Slip Speed Estimator

The slip of an induction machine is the difference between its synchronous speed and rotor speed. At standstill, the slip is 100%, and at the rated frequency, it can be generally 2–5%. To develop the torque by an induction machine, it needs to generate the slip. As the synchronous frequency becomes smaller in the low-speed region, the slip cannot be neglected and needs to be compensated adequately; otherwise, the motor will not be able to develop the sufficient torque to drive the load. The slip ω_{sl} is estimated from the motor torque, T_e. The estimation is done in rotor-flux-oriented frame. The torque and the slip are related as shown in Eq. (3).

$$T_e = \left(\frac{n_p}{R_r}\right)(i_{ds}^r)^2 L_m^2 \omega_{sl}, \tag{3}$$

where L_m = magnetizing inductance, R_r = rotor resistance and the slip speed ω_{sl} can be estimated in Eq. (4):

$$\omega_{sl} = \frac{T_e R_r}{n_p L_m^2 (i_{ds}^r)^2}. \tag{4}$$

In order to implement Eq. (4), the stator current in rotor-flux-oriented frame must be known. In the decoupling control action, the stator current is decoupled in flux and torque component in rotor-flux-oriented frame. For this, the stator current in stator reference frame is converted into rotor-flux-oriented frame. This is done with the help of vector relational operator (vector rotator (VR) or unit vector). It is defined by $e^{j\theta}$. The vector rotator converts the rotating frame variables into stationary frame variables, and $\cos\theta$ and $\sin\theta$ are the Cartesian components of unit vectors. The $e^{-j\theta}$ is defined as inverter vector rotator (VR^{-1}) that converts stationary frame variables into rotating frame variables. The angle θ is the angle

associated with the reference frame into which the conversion is being made. Here, in this case, the stationary frame variables are converted to rotating frame variables, and the sine and cosine of the rotor-flux-oriented frame can be obtained by Eq. (5) as follows:

$$\left.\begin{array}{l} \cos\theta_{\Psi_r} = \dfrac{\Psi_{dr}^s}{\widehat{\Psi_r}} \\[2mm] \sin\theta_{\Psi_r} = \dfrac{\Psi_{qr}^s}{\widehat{\Psi_r}} \end{array}\right\}, \tag{5}$$

where

$$\Psi_{dr}^s = \frac{L_r}{L_m}\left(\Psi_{ds}^s - \sigma L_s i_{ds}^s\right) \quad L_r = rotor\ inductance,$$

$$\Psi_{qr}^s = \frac{L_r}{L_m}\left(\Psi_{qs}^s - \sigma L_s i_{qs}^s\right),$$

$$\widehat{\Psi_r} = \sqrt{\left(\Psi_{dr}^s\right)^2 + \left(\Psi_{qr}^s\right)^2}.$$

Now, with the help of Park transformation, the flux and torque component of stator current in rotor-flux-oriented frame can be obtained as shown in Eqs. (6) and (7):

$$i_{ds}^r = i_{ds}^s \cos\theta_{\Psi_r} + i_{qs}^s \sin\theta_{\Psi_r}, \tag{6}$$

$$i_{qs}^r = -i_{ds}^s \sin\theta_{\Psi_r} + i_{qs}^s \cos\theta_{\Psi_r}. \tag{7}$$

Thus, from the above estimations, the electromagnetic torque, T_e, and the flux component of stator current, i_{ds}^r, are obtained. So, with the help of Eq. (4), the slip speed ω_{sl} can be found. The block diagram for slip speed estimation is shown in Fig. 4.

The motor stator terminals three-phase voltages and currents are sensed and, through Clark's transformation, converted into stationary two-axis components, i.e. direct axis and quadrature axis (dq axis). The torque is estimated
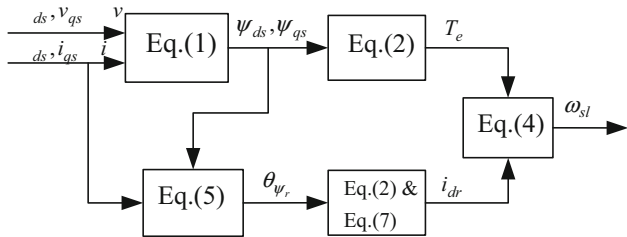
Fig. 4 Slip speed estimation block diagram

from Eq. (2). With the help of Park transformation, the stator current in stationary reference frame is converted into rotor-flux-oriented frame variables. This allows the decoupling of stator current into two parts, responsible for flux and torque components. With the known values of torque and stator current in rotor-oriented frame, the slip speed is estimated which in turn further added to reference speed command to generate synchronous speed. In the next process, the *V/f* control is applied to generate three-phase sinusoidal reference signals for nine-level asymmetrical inverter. For the scheme to run successfully with proposed asymmetrical inverter structure, the induction motor should have isolated winding (IW) or open-end windings.

3 Simulation and Experimental Results

The simulation results are produced using MATLAB 7.10 (2008a) in co-simulation with PSIM7.05 for modelling the isolated winding (IW) induction motor. The solver discrete (with no continuous states) with fixed step solver type along with 40 µs fixed step size is chosen in MATLAB/ SIMULINK configuration parameter. The control scheme comprising stator flux estimation, motor torque estimation, stationary frame variable to rotary frame variable conversion, slip speed estimation, open-loop constant *V/f* control and three-phase reference signal generation and nearest level control modulation strategy is simulated in MATLAB software.

To fulfil the requirement of variable DC link voltages ($3V_{dc}$ and V_{dc}) for MAIN and AUX inverters, input supply to the DC–DC converter (V_s) is considered as 200 V with carrier frequency as 12 kHz and the DC supply voltage (V_s) is adjusted through the DC–DC converter. Hardware set-up of 5 kW, nine-level asymmetrical MLI is built for laboratory purpose to drive an IM (three phases) of rating 1 HP, 200 V, 50 Hz. Simulation and experimental parameters along with the component specifications are mentioned in "Appendix".

In Fig. 5, the speed command is kept at $\omega_{ref} = 100$ RPM (3.33 Hz). In Fig. 5a, b, the voltage and current waveforms are still distorted, but in voltage waveform, the nine-level
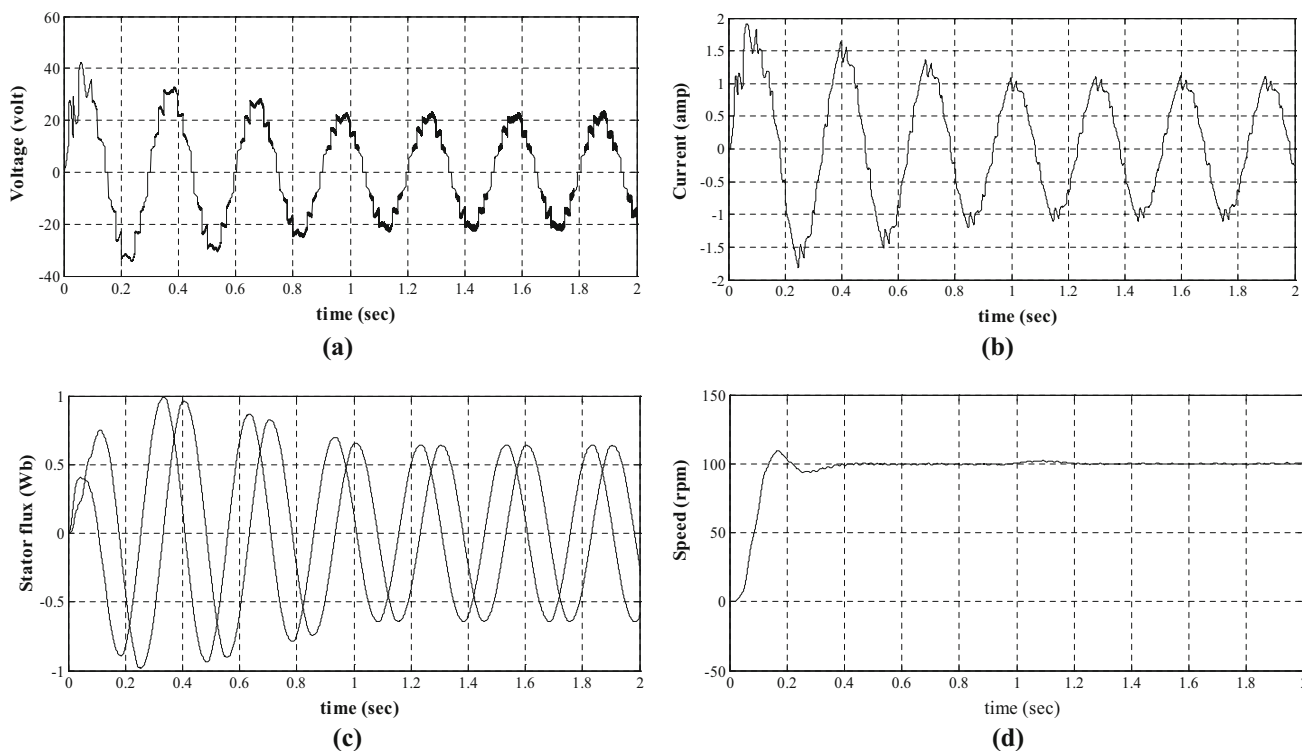

Fig. 5 Simulation results at 100 RPM: **a** stator terminal one-phase voltage. **b** Stator one-phase current. **c** Stator dq-axis flux. **d** Speed
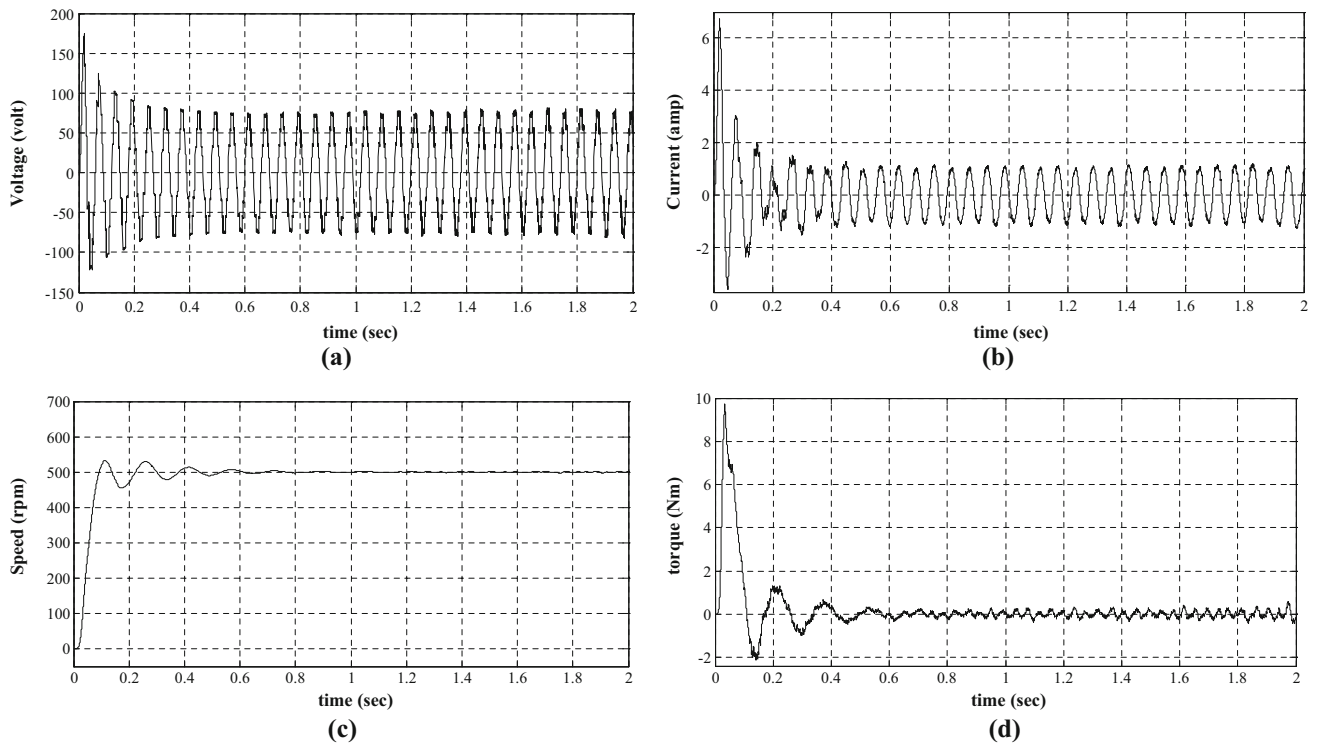
Fig. 6 Simulation results at 500 RPM: **a** stator terminal one-phase voltage. **b** Stator one-phase current. **c** Speed. **d** Torque
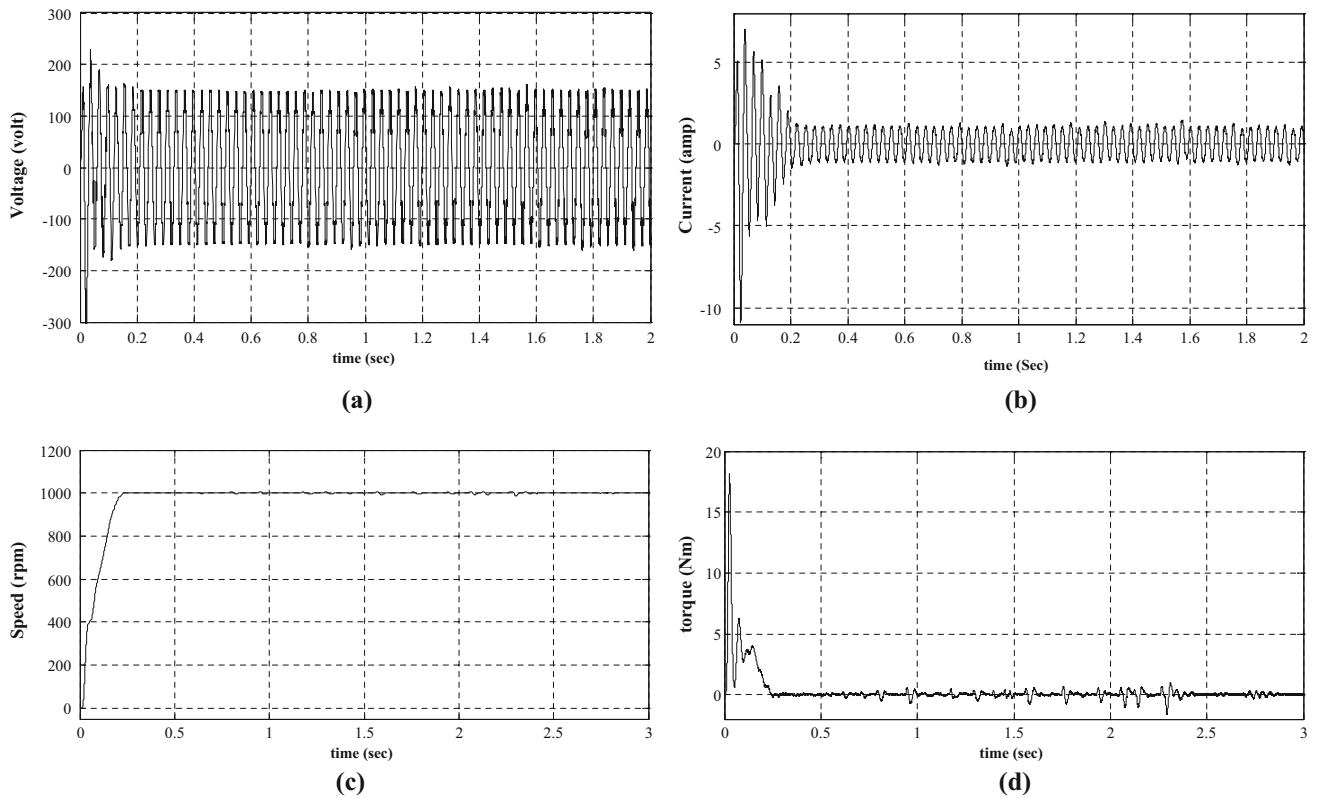

Fig. 7 Simulation results at 1000 RPM: **a** stator terminal one-phase voltage. **b** Stator one-phase current. **c** Speed. **d** Torque
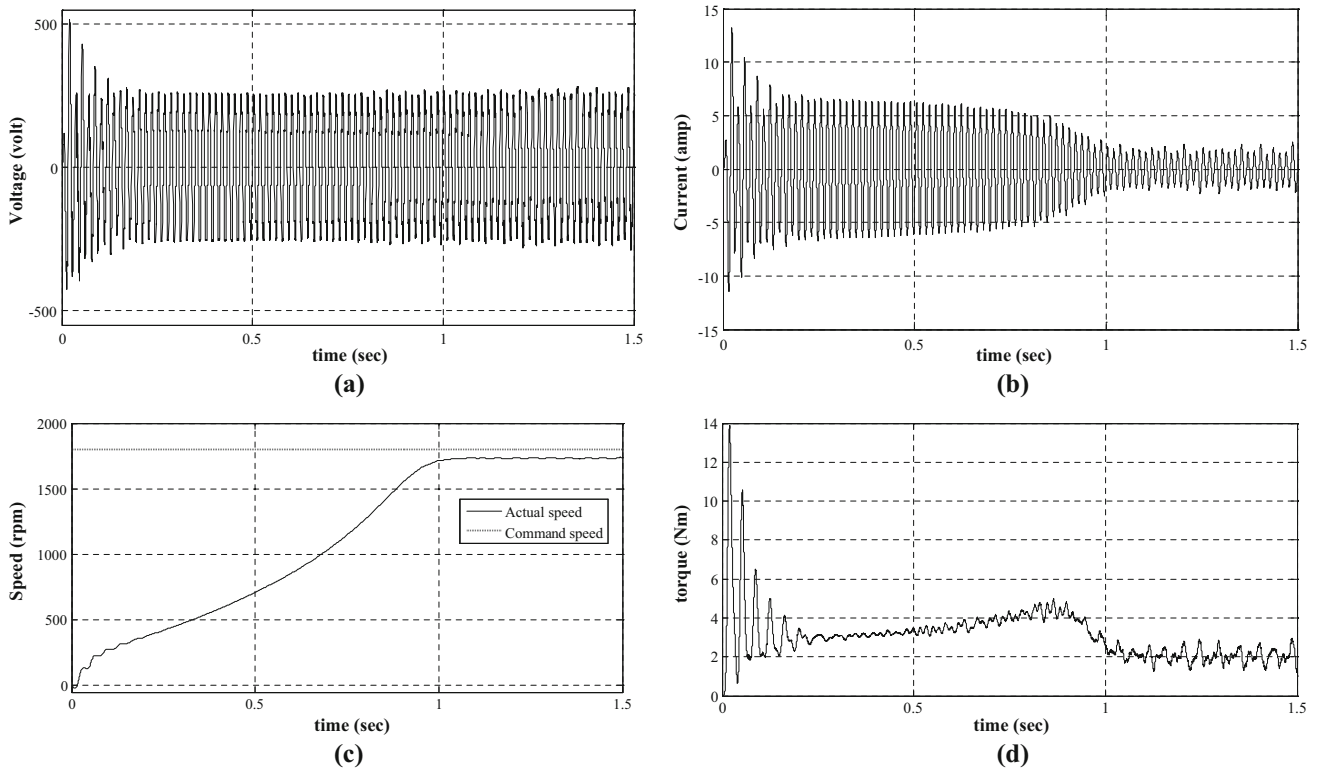
Fig. 8 Simulation results at speed 1800 RPM: **a** stator R-phase voltage. **b** R-phase current. **c** Speed. **d** Torque at 2 Nm
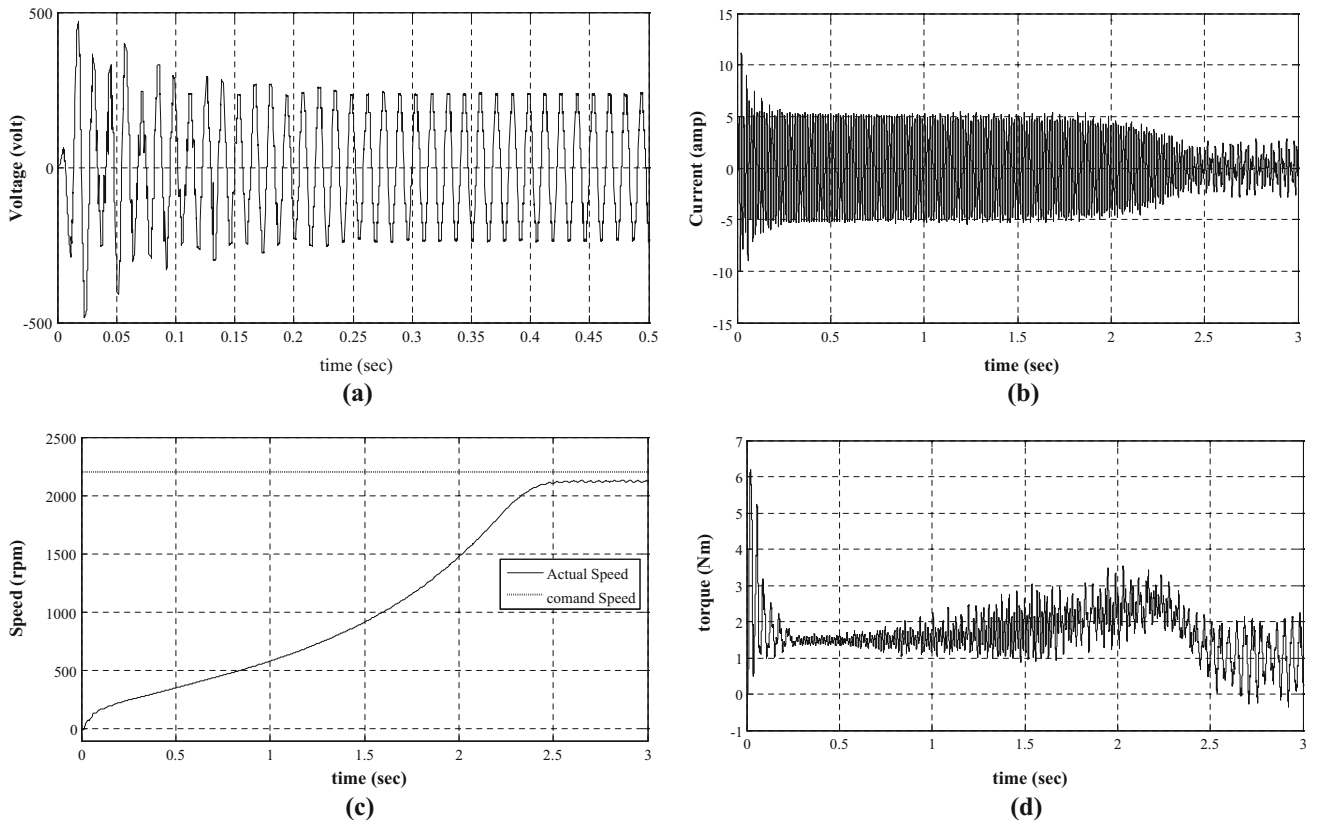

Fig. 9 Simulation results at speed 2200 RPM: **a** stator R-phase voltage. **b** R-phase current. **c** Speed. **d** Torque at 1 Nm
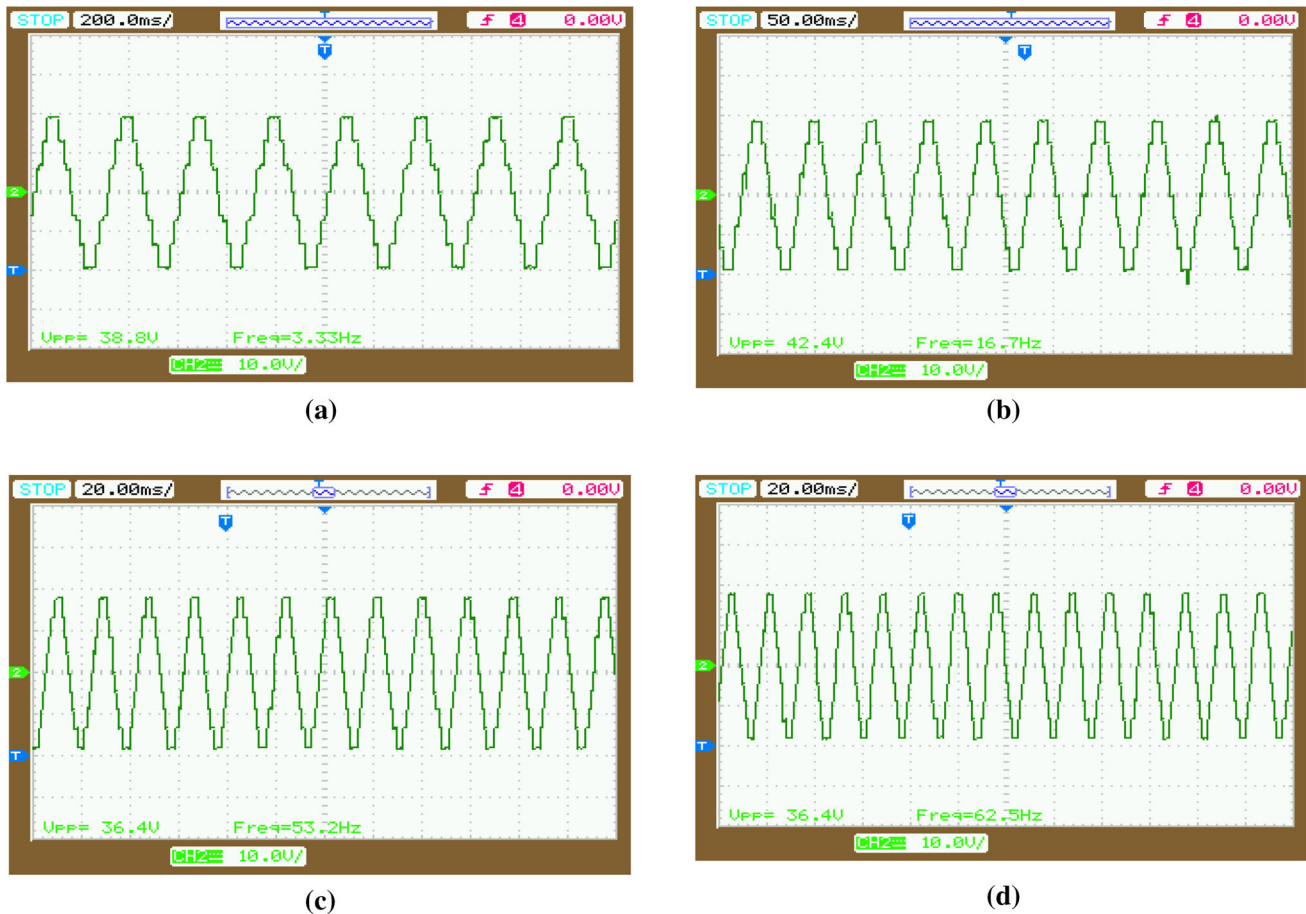
(a)

(b)

(c)

(d)

Fig. 10 Experimental results for only frequency control at below base speed: **a** 100 RPM. **b** 500 RPM and at above base speed: **c** 1600 RPM. **d** 1800 RPM

output voltage can be counted easily. The ripples in speed are much less in the range of 3–5 RPM as shown in Fig. 5c, d. The stator dq-axis fluxes are 0.75 Wb and frequency changes as per the input speed command.

In Fig. 6, simulation results are recorded for the speed command of $\omega_{ref} = 500$ RPM (16.67 Hz). Figure 6a, b clearly depicts that the voltage and current waveforms are improved, respectively. Figure 6c shows that after some speed transients, the rotor speed almost becomes ripples free. The torque waveform also contains lesser ripples as shown in Fig. 6d.

Figure 7 shows the simulated waveforms at $\omega_{ref} = 1000$ RPM (33.33 Hz). In Fig. 7c, there is an almost negligible overshoot in the speed waveform and it is almost ripple free. The stator terminal R-phase voltage and current waveforms are non-comparably improved and are almost sinusoidal, varying as shown in Fig. 7a, b. The torque waveform with lesser ripples is also shown in the last in Fig. 7d.

It can be stated from Figs. 5, 6 and 7 that, except the low-speed command up to 35–30 Hz, the transient conditions for the waveforms recorded are good and for all the

speed command from 1 to 50 Hz, the motor runs very smoothly during steady-state period. All the waveforms have values well within the safe limits. The simulation results are shown for the induction motor at different speed commands from very low speed, i.e. 100 RPM (3.33 Hz) to base speed 1000 RPM (33.33 Hz), but through the proposed control scheme, the motor can be driven well beyond the base speed.

Figure 8 presents the simulation results for the motor speed above rated speed command. The reference speed, this time, is set to $\omega_{ref} = 1800$ RPM (60 Hz). It is clear from the well-known fact that from zero speed up to base speed, motor is controlled under constant V/f control mode which means up to base speed, motor flux remains constant. But, above base speed, the applied voltage to motor is limited to rated value and only frequency is varied further, which brings motor to flux-weakening mode. In Fig. 8a, the voltage becomes constant at rated value but its frequency is changed according to the speed command. The current waveform is shown in Fig. 8b. The motor takes up to 1 s time to follow the command speed but with a different speed other than command speed due to the
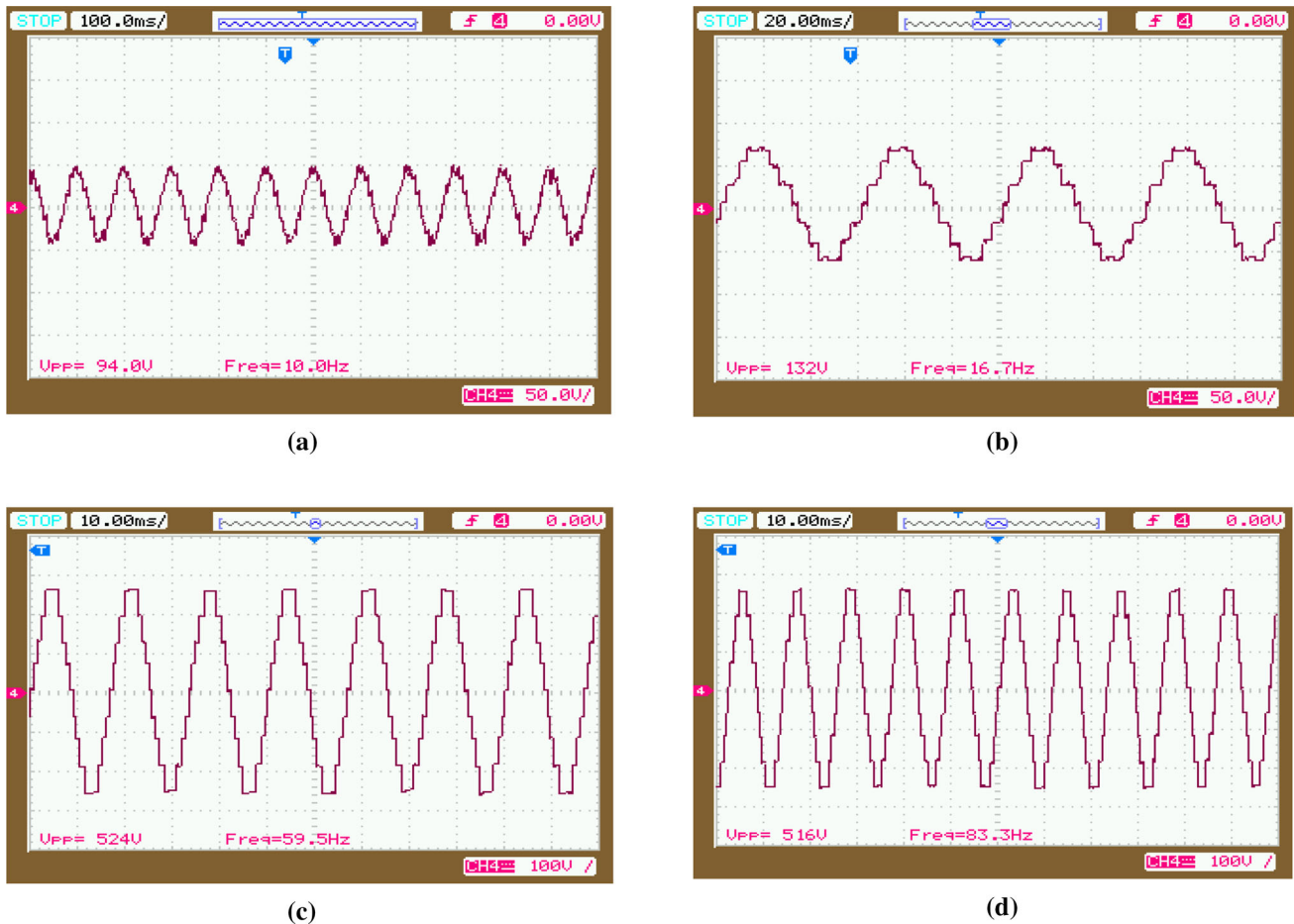
Springer

Fig. 11 Experimental results for constant *V/f* control at below base speed: **a** 100 RPM. **b** 500 RPM and at above base speed: **c** 1800 RPM. **d** 2500 RPM

Fig. 12 Complete circuit test bench in laboratory

application of constant load torque (2Nm) as explained earlier and is depicted in Fig. 8c. Again as depicted in Fig. 8d, the torque waveform has the ripples within the range of + 1 to − 1 Nm.

In Fig. 9, the motor is given a speed command of $\omega_{ref} =$ 2200 RPM (73.33 Hz) with an application of load torque of 1Nm. As the motor flux weakens more, it takes more time

(approximately 2.5 s) to develop the speed. With the application of continuous torque of 1Nm, the motor does not follow the commanded speed exactly. The motor terminal voltage is fixed at rated value as in Fig. 9a at higher frequency as decided by the command speed. Current is well within the safe limits as in Fig. 9b. In Fig. 9c, the speed curve has a dip during the starting period. This is because of the application of load torque from the very start to motor and motor needs enough time to develop the sufficient slip to drive the load. Once it develops the sufficient torque due to production of sufficient slip, it builds the full speed as ordered by command speed. The torque waveform shown in Fig. 9d still has the ripples in the range of 0–2Nm.

For only frequency control, the motor terminal voltage is kept fixed and does not change at different speed commands. This type of control provides a wide range of speed control of induction motor, but this mode of operation leads motor into flux-weakening mode. In Fig. 10a–d, the results are shown for only frequency control speed command at below base speed (100 and 500 RPM) as well as
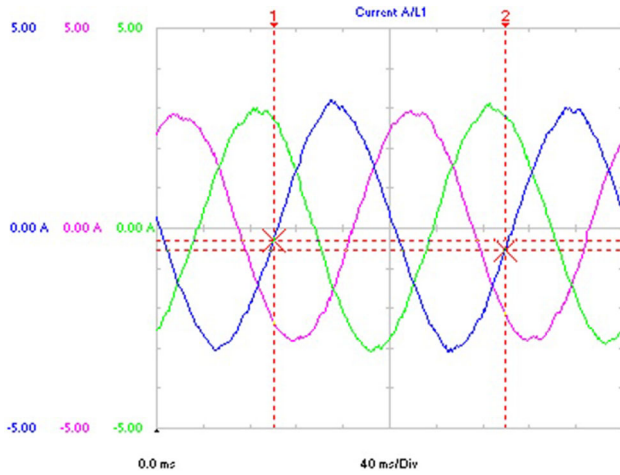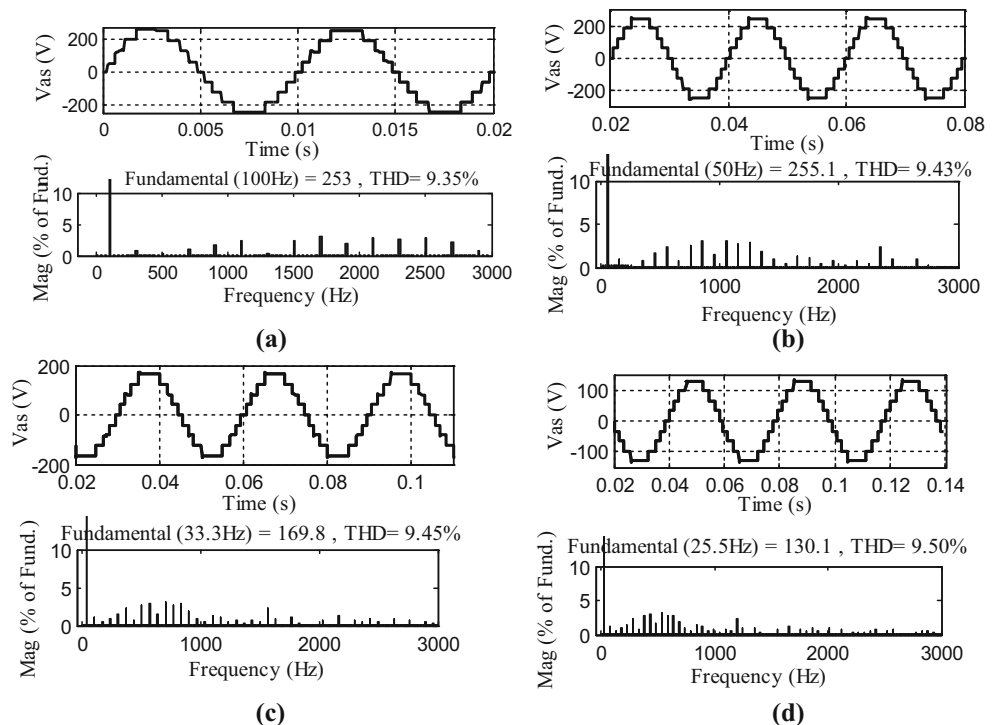
Fig. 13 Experimental result of proposed nine-level inverter current at a motor speed of 800 RPM. Current A/L1: X scale = 40 ms/Div; Y scale = 5 A/Div; maximum = 3.22 A; minimum = −3.09 A. Current B/L2: X scale = 40 ms/Div; Y scale = 5 A/Div; maximum = 3.22 A; minimum = −3.09 A. Current C/L3: X scale = 40 ms/Div; Y scale = 5 A/Div; maximum = 3.22 A; minimum = −3.09 A. Cursor values of current A/L1: $X1$ = 20 ms; $X2$ = 59.8 ms; dX = 39.8 ms. $Y1$ = −0.32 A; $Y2$ = −0.55 A; Dy = −0.23 A

above base speed (1600 and 1800 RPM), respectively. In all the voltage waveforms for the different speed commands, the number of voltage levels remains constant and therefore the nine levels in output voltage are distinctly visible.

For constant V/f control, the motor flux is constant from low-speed region up to rated speed as the V/f ratio is maintained constant. This helps the motor to develop the rated torque at each speed up to base speed. Beyond the base speed, voltage is restricted to rated value and only the frequency is varied. Above rated speed, the motor operates in flux-weakening mode. Experimental results for constant V/f control at below base speed (100 and 500 RPM) as well as above base speed (1800 and 2500 RPM) is shown in Fig. 11a–d, respectively.

In Fig. 12, the complete inverter hardware set-up driving the 1 HP induction motor load is shown. The input to the inverter is given through the power rectifier module which takes the three-phase AC mains as the input. An auto transformer is inserted between the AC mains and rectifier to supply the controlled DC to the inverter. Figure 13 shows the experimental result of proposed nine-level inverter current at a motor speed of 800 RPM. Three-phase stator current at 800 RPM (frequency is 25.5 Hz) is measured and analysed so that the stator currents are nearly balanced and sinusoidal in nature. Figure 14 shows the simulation results of output phase voltage along with total harmonic distortion (%THD) at different speeds of: (a) 3000 RPM, (b) 1500 RPM, (c) 1000 RPM and (d) 800 RPM using V/f control. It is easily observed that the number of inverter output voltage levels remained the same along with %THD of approximately 9% irrespective of the reference magnitude of the voltage or the speed.

Fig. 14 Simulation results of phase voltage of proposed nine-level inverter using V/f control of induction motor at various speeds of: **a** 3000 RPM, **b** 1500 RPM, **c** 1000 RPM, **d** 800 RPM

4 Conclusion

Cascaded nine-level inverter having different values of input DC voltage source is designed for laboratory prototype. DC–DC converter is employed to achieve constant output voltage levels and harmonics, and nearest level modulation strategy is presented where inverter frequency is varied to control the DC link voltage irrespective of reference voltages. It is understood that from zero to base speed, motor can be controlled under constant V/f control mode and the motor flux remains constant up to base speed, whereas at above base speed, motor can be controlled under only frequency control and motor runs in flux-weakening mode. The simulation results are shown for the induction motor at different speed commands from very low speed, i.e. 100 RPM (3.33 Hz) to base speed 1000 RPM (33.33 Hz). It is worth mentioning from the results obtained from simulation and experimental test bench that at different speeds (above base speed as well as below base speed), the isolated winding or open-end winding induction motor can be driven well with constant voltage level and harmonics with a THD of approximately 9%.

Appendix

See Table 1.

Table 1 Components and their specification for experimental prototype and simulation purposes

Components	Ratings/specifications
Input DC supply voltage of the DC–DC converter, V_s	200 V
Maximum DC link voltage of MAIN inverter, $V_{DC} = 3V_{dc}$	190 V
Maximum DC link voltage of AUX inverter, V_{dc}	63.3 V
Multiwinding step-down transformer rating	1 kVA, 200/66 V
IGBT for DC–DC converters and inverters (MAIN inverters and inverters of AC link system)	K75T60 (600 V, 75A)
Rating of the capacitor in DC–DC converter	470 mF, 415 V
Rating of the inductor in DC–DC converter	150 mH
P-MOSFET for AUX inverters	IRFP460 (500 V, 20 A)
Rating of the capacitor in auxiliary inverters	450 mF, 415 V
Open-end winding induction motor	1 HP, 200 V, 50 Hz
Switching frequency of IGBT for the DC–DC converter	12 kHz
Switching frequency of IGBT for the AC link inverter	3 kHz
Proportional gain of the voltage controller, K_p	10
Integral gain of the voltage controller, K_i	0.1

References

Abu-rub H, Holtz J, Rodriguez J, Baoming G (2010) Medium-voltage multilevel converters—State of the art, challenges, and requirements in industrial applications. IEEE Trans Ind Electron 57(8):2581–2596

Al-Othman AK, Abdelhamid TH (2009) Elimination of harmonics in multilevel inverters with non-equal dc sources using PSO. Energy Convers Manag 50(3):756–764

Babaei E, Moeinian MS (2010) Asymmetric cascaded multilevel inverter with charge balance control of a low resolution symmetric subsystem. Energy Convers Manag 51(11):2272–2278

Banaei MR, Salary E (2011) New multilevel inverter with reduction of switches and gate driver. Energy Convers Manag 52(2):1129–1136

Bhuvaneswari G, Nagaraju (2005) Multi-level inverters—a comparative study. IETE J Res 51(2):141–153. https://doi.org/10.1080/03772063.2005.11416389

Boby M, Pramanick S, Kaarthik RS, Rahul SA, Gopakumar K, Umanand L (2016) Multilevel dodecagonal voltage space vector structure generation for open-end winding IM using a single DC source. IEEE Trans Ind Electron 63(5):2757–2765

Cheng Y, Qian C, Crow ML, Pekarek S, Atcitty S (2006) A comparison of diode-clamped and cascaded multilevel converters for a STATCOM with energy storage. IEEE Trans Ind Electron 53(5):1512–1521

Chowdhury S, Wheeler P, Patel C, Gerada C (2016) A multi-level converter with a floating bridge for open-ended winding motor drive applications. IEEE Trans Ind Electron 63(9):5366–5375

Colak I, Kabalci E, Bayindir R (2011) Review of multilevel voltage source inverter topologies and control schemes. Energy Convers Manag 52(2):1114–1128

Dahidah MSA, Konstantinou G, Agelidis VG (2015) A review of multilevel selective harmonic elimination PWM: formulations, solving algorithms, implementation and applications. IEEE Trans Power Electron 30(8):4091–4106

Deng Y, Harley RG (2015) Space-vector versus nearest-level pulse width modulation for multilevel converters. IEEE Trans Power Electron 30(6):2962–2974

Dixon J, Morán L (2005) A clean four-quadrant sinusoidal power rectifier using multistage converters for subway applications. IEEE Trans Ind Electron 52(2):653–661

Dixon J, Pereda J, Castillo C, Bosch S (2010) Asymmetrical multilevel inverter for traction drives using only one DC supply. IEEE Trans Veh Technol 59(8):3736–3743

Edpuganti A, Rathore AK (2015) New optimal pulsewidth modulation for single DC-link dual inverter fed open-end stator winding induction motor drives. IEEE Trans Ind Electron 30(8):4386–4393

Franquelo LG, Rodriguez J, Leon JI, Kouro S, Portillo R, Prats MAM (2008) The age of multilevel converters arrives. IEEE Ind Electron Mag 2(2):28–39

Hosseinzadeh MA, Farhadi KM, Babaei E (2013) Asymmetrical multilevel converter topology with reduced number of components. IET Power Electron 6(6):1188–1196

Hu P, Jiang D (2015) A level-increased nearest level modulation method for modular multilevel converters. IEEE Trans Power Electron 30(4):1836–1842

Jana KC, Biswas SK (2015) Generalised switching scheme for a space vector pulse-width modulation-based N-level inverter with reduced switching frequency and harmonics. IET Power Electron 8(12):2377–2385

Jana KC, Biswas S, Chowdhury SK (2016) Dual reference phase shifted PWM technique for a N-level inverter based grid

connected solar photovoltaic system. IET Renew Power Gener 10(7):928–935

Krug D, Bernet S, Fazel SS, Jalili K, Malinowski M (2007) Comparison of 2.3-kV medium-voltage multilevel converters for industrial medium-voltage drives. IEEE Trans Ind Electron 54(6):2979–2992

Lai JS, Peng FZ (1996) Multilevel converters—a new breed of power converters. IEEE Trans Ind Appl 32(3):509–517

Lezana P, Ortiz G (2009) Extended operation of cascade multicell converters under fault condition. IEEE Trans Ind Electron 56(7):2697–2703

Li W, He X, Hu J et al (2016) Common-mode voltage injection-based nearest level modulation with loss reduction for modular multilevel converters. IET Renew Power Gener 10(6):798–806

Lu S, Mariéthoz S, Corzine KA (2010) Asymmetrical cascade multilevel converters with noninteger or dynamically changing DC voltage ratios: concepts and modulation techniques. IEEE Trans Ind Electron 57(7):2411–2418

Luo H, Wang Q, Deng X, Wan S (2006) A novel V/f scalar controlled induction motor drives with compensation based on decoupled stator current. In: Proceedings of the IEEE international conference on industrial technology, pp 1989–1994

Mahato B, Thakura PR, Jana KC (2014) Hardware design and implementation of unity power factor rectifiers using microcontrollers. In: IEEE 6th India international conference on power electronics, India, pp 1–5

McGrath BP, Holmes DG (2002) Multicarrier PWM strategies for multilevel inverters. IEEE Trans Ind Electron 49(4):858–867

Malekjamshidi Z, Jafari M, Islam R, Zhu J, Member, S (2014) A comparative study on characteristics of major topologies of voltage source multilevel inverters. In: Innovative smart grid technologies—Asia (ISGT Asia), pp 612–617

Meshram PM, Borghate VB (2015) A simplified nearest level control (NLC) voltage balancing method for modular multilevel converter (MMC). IEEE Trans Power Electron 30(1):450–462

Naderi R, Rahmati A (2008) Phase-shifted carrier PWM technique for general cascaded inverters. IEEE Trans Power Electron 23(3):1257–1269

Perez M, Rodriguez J, Pontt J, Kouro S (2007) Power distribution in hybrid multi-cell converter with nearest level modulation. In: IEEE international symposium industrial electronics, pp 736–741

Pramanick S, Azeez NA, Kaarthik RS, Gopakumar K, Cecati C (2015) Low-order harmonic suppression for open-end winding IM with dodecagonal space vector using a single DC-link supply. IEEE Trans Ind Electron 62(9):5340–5347

Rathore A, Edpuganti A (2015) Optimal low switching frequency pulsewidth modulation of nine-level cascade inverter. IEEE Trans Power Electron 30(1):482–495

Rech C, Pinheiro JR (2007) Hybrid multilevel converters: unified analysis and design considerations. IEEE Trans Ind Electron 54(2):1092–1104

Rodríguez J, Lai JS, Peng FZ (2002) Multilevel inverters: a survey of topologies, controls, and applications. IEEE Trans Ind Electron 49(4):724–738

Rodríguez J, Bernet S, Wu B, Pontt JO, Kouro S (2007) Multilevel voltage-source-converter topologies for industrial medium-voltage drives. IEEE Trans Ind Electron 54(6):2930–2945

Rodríguez J, Franquelo LG, Kouro S, Leon JI, Portillo RC, Prats MAM, Perez MA (2009) Multilevel Converters: an enabling technology for high-power applications. Proc IEEE 97(11):1786–1817

Ruiz-Caballero D, Martinez L, Ramos AR, Mussa SA (2009) New asymmetrical hybrid multilevel voltage inverter. In: Brazilian power electron conference, pp 354–361

Son GT, Lee HJ, Nam TS et al (2012) Design and control of a modular multilevel HVDC converter with redundant power modules for noninterruptible energy transfer. IEEE Trans Power Deliv 27(3):1611–1619

Sudharshan KR, Gopakumar K, Mathew J, Undeland T (2015) Medium-voltage drive for induction machine with multilevel-dodecagonal voltage space vectors with symmetric triangles. IEEE Trans Ind Electron 62(1):79–87

Sudheer P, Prasad KRS (2014) H-bridge multi level under different loads. Int J Sci Res Publ 4(5):1–5

Vazquez S, Leon JI, Franquelo LG, Padilla JJ, Carrasco JM (2009) DC-voltage-ratio control strategy for multilevel cascaded converters fed with a single DC source. IEEE Trans Ind Electron 56(7):2513–2521

Wang C-C, Fang C-H (2003) Sensorless scalar-controlled induction motor drives with modified flux observer. IEEE Trans EnergyConvers 18(2):181–186

Wen J, Smedley KM (2008) Synthesis of multilevel converters based on single- and/or three-phase converter building blocks. IEEE Trans Power Electron 23(3):1247–1256

Xiong C-L, Feng X-Y, Diao F, Wu X-J (2016) Improved nearest level modulation for cascaded H-bridge converter. Electron Lett 52(8):648–650